PHOTONICS Research

Improved common-path spectral interferometer for single-shot terahertz detection

Shuiqin Zheng,[1,2] Qinggang Lin,[1] Yi Cai,[1] Xuanke Zeng,[1,2] Ying Li,[2] Shixiang Xu,[1,*] Jingzhen Li,[1] and Dianyuan Fan[2]

[1]Shenzhen Key Laboratory of Micro-Nano Photonic Information Technology, College of Electronic Science and Technology, Shenzhen University, Shenzhen 518060, China
[2]SZU-NUS Collaborative Innovation Center for Optoelectronic Science & Technology, Key Laboratory of Optoelectronic Devices and Systems of Ministry of Education and Guangdong Province, Shenzhen University, Shenzhen 518060, China
*Corresponding author: shxxu@szu.edu.cn

Received 5 January 2018; accepted 8 January 2018; posted 10 January 2018 (Doc. ID 319065); published 14 February 2018

To seek high signal-to-noise ratio (SNR) is critical but challenging for single-shot intense terahertz (THz) coherent detection. This paper presents an improved common-path spectral interferometer for single-shot THz detection with a single chirped pulse as the probe for THz electro-optic (EO) sampling. Here, the spectral interference occurs between the two orthogonal polarization components with a required relative time delay generated with only a birefringent plate after the EO sensor. Our experiments show that this interferometer can effectively suppress the noise usually suffered in a non-common-path interferometer. The measured single-shot SNR is up to 88.85, and the measured THz waveforms are independent of the orientation of the used ZnTe EO sensor, so it is easy to operate and the results are more reliable. These features mean that the interferometer is quite qualified for applications where strong THz pulses, usually with single-shot or low repetition rate, are indispensable.

OCIS codes: (040.2235) Far infrared or terahertz; (320.7100) Ultrafast measurements; (230.2090) Electro-optical devices; (300.6495) Spectroscopy, terahertz; (120.3180) Interferometry.

https://doi.org/10.1364/PRJ.6.000177

1. INTRODUCTION

In recent years, intense terahertz (THz) fields have drawn more and more attention because of their many applications in extreme THz science featuring strong THz light–matter interactions, nonlinear spectroscopy, and imaging [1]. Correspondingly, coherent detection for the THz intense field has also become a hot topic in THz communities. THz electro-optic sampling (THz-EOS) has long been an important tool because of its ability to simultaneously detect both the amplitude and phase of a THz field with broad bandwidth, besides its simple alignment [2]. However, traditional THz-EOS is invalid if the target THz field is not weak enough [3,4]. For strong THz electric fields, it will not only result in deformed waveforms, but it will also result in "over-rotation" and ambiguity [5]. Additionally, the intense THz field usually works with a low repetition rate or single-shot mode, which means the traditional THz-EOS, operating usually with a pump-probe mode, also cannot work well [6]. As a result, many activities have been motivated to develop qualified single-shot THz detection. Spectral encoding was first used to implement single-shot THz-EOS with a chirped pulse to provide a mapping between time and wavelength [7]. Regretfully, it was plagued by a loss of temporal resolution due to its simple time-wavelength mapping approximation and also by its validity for only the weak THz field because it works on polarization-sensitive intensity modulation. Some other efforts for single-shot THz detection include angle-to-time encoding with transmissive dual echelons [8,9] and a time-space encoding method by non-collinear crossing, echelon mirrors, or by pulse-front tilting [10–15]. In spite of the successes, all the single-shot detections mentioned above work on the polarization-sensitive intensity modulation, and thereby still fail to get rid of the weak-field limitation. Some reports have proved that THz detection with spectral interferometry can overcome the weak-field limitation by easily unwrapping the measured phase changes with some simple algorithms [16,17]. Unfortunately, the highly sensitive interferometric measurement requires stringent experimental conditions for accurate implementation because the fidelity of the fringes is only maintained for collinear beams with high optical phase stability and good spatial beam mode matching [6]. Sharma *et al.* [18] tried to realize self-referenced spectral interferometric measurements by subtracting the phase measured at the edge of the probe beam from the phase values of the center of the beam in order to effectively avoid the stringent

experimental conditions and thereby promote the measured signal-to-noise ratio (SNR) sixfold, but it cannot operate in single-shot mode.

In order to get high SNR of single-shot THz coherent detection for the intense THz field, we have recently demonstrated theoretically and experimentally a common-path spectral interferometer (CP-SI) for single-shot THz electro-optics detection [19]. Its common-path alignment can be effectively immune to the disturbances from environment, e.g., vibrations, air turbulences, and temperature fluctuations, and can thus improve the measured SNR by about 5.2 times compared with the conventional Mach–Zehnder spectral interferometer (MZ-SI). However, this design can record THz waveforms without deformation only when α, the angle between the polarization of the normally incident THz field and the [0,0,1] axis of the used (110) ZnTe-EO sensor, is equal to 0° or 180°. This implies that α must be carefully calibrated before measurements. Here, we present an improved CP-SI for single-shot THz detection to avoid the α-dependence of the recorded waveforms. Furthermore, this improvement can enhance the measured signal by a factor of ∼1.8, which means the measured SNR can be 1.8 times higher than that with the previous design for the same target signals.

2. EXPERIMENTAL SETUP AND DESCRIPTION

Figure 1 shows the setup of our improved CP-SI. Here, the used laser source is a 1-kHz, 35-fs, 800-nm Ti:sapphire amplifier that can output a pulse chain with an average power up to 3.5 W. About 2.0 W of the pulse chain reaches a $LiNbO_3$ crystal as the pump via the tilted-pulse-front technique to generate THz radiation [20], the target THz field of all following measurements. The beam used as probe is about 20 mW. A beam sampler is used to reflect a small part of the probe (∼1 mW) for characterizing the temporal/spectral phase of the probe in real time by our homemade spectral phase interferometer for direct electrical field reconstruction (SPIDER) [21]. The transmission of the sampler then passes through a stretcher, including a pair of 180° folding right-angle SF57 prisms, to be stretched up to 12 ps, which is long enough to temporally cover the target THz field. This arrangement allows us to realize single-shot operation by the aid of a pulse selector. An achromatic half-wave plate (AHWP) is set next to the pulse stretcher to rotate the probe polarization by about 45° with regard to horizontal polarization. A 1-mm-thick ⟨110⟩ ZnTe-EO crystal (EOC) is aligned with an angle of 120° between the [0,0,1] axis and the vertical direction for maximizing the measured THz signal. After the EOC, a 2.4-mm-thick α–barium-borate (BBO) plate with its optical axis in its surfaces and along the horizontal direction is used in order to get a relative time delay τ (∼1 ps) between the two orthogonally polarized components of the probe beam for proper spectral interference fringes. Then a polarizer is followed with an angle of ∼45° between its polarization axis and the polarization directions of the two components so that the recorded spectral interferogram has maximal optical modulation. Here the used spectrometer is a fiber spectrometer (HR4000, Ocean Inc., 1 × 3648 pixels) with a resolution of 0.1 nm from 720 to 880 nm. Moreover, setups for original CP-SI and MZ-SI are the same as in Ref. [19].

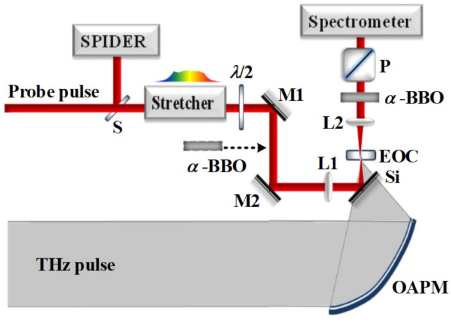

Fig. 1. Experimental setup. S, sampler; M1 ∼ M3, mirrors; L1, 2, lenses; EOC, ⟨110⟩ ZnTe EO crystal; Si, silica wafer; BS1, 2, beam splitters; OAPM, off-axial parabolic mirror; SPIDER, spectral phase interferometer for direct electrical field reconstruction; P, polarizer.

Obviously, here the THz signal is probed by single beam based on the THz EO effect. The recorded spectral interference occurs between two beams, which are two components of the identical probe beam with orthogonal polarization states. The required relative time delay between the components for spectral interference is induced by simply inducing a transmissive birefringent plate after the EOC. As a result, the two beams involved in spectral interferometry propagate always along the common path, which is very helpful to suppress the noise during our measurements. The ⟨110⟩ ZnTe crystal is used here as the THz EO sensor because it can provide good phase matching between the 800-nm ultrashort pulses and THz field and has commercial quality.

In fact, the final received spectral interferogram of spectrometer derives from interference between the ordinary light and the extraordinary light of the α-BBO plate. The system measures the additional phase difference from the THz field between the two lights, so the two lights can be seen as two probes in the EOC. As shown in Fig. 2, when the angle between the normally incident THz field and the [0,0,1] axis of the EOC is equal to α, according to Ref. [22], the refractive index variations imposed by THz field along the orthogonal directions z'' and y'' can be expressed as

$$\Delta n_{z''} = \frac{n^3}{2} E_{\mathrm{THz}}(t) r_{41} [\cos\alpha \cos^2\theta - \cos(\alpha + 2\theta)], \quad (1)$$

and

$$\Delta n_{y''} = \frac{n^3}{2} E_{\mathrm{THz}}(t) r_{41} [\cos\alpha \sin^2\theta + \cos(\alpha + 2\theta)], \quad (2)$$

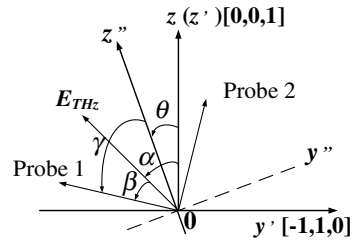

Fig. 2. Geometry of THz EO detection based on ⟨110⟩ ZnTe crystal. The plane of the page is the (110) plane of the crystal, and the angles α and θ are measured inside the (110) plane.

with $\tan(2\theta) = -2\tan\alpha$. Here, the parameters n and r_{41} stand for the refractive index and the EO tensor, while θ and β represent the angles between z'' and the [0,0,1] axis and between the probe beam polarization and the [0,0,1] axis as shown in Fig. 2. Accordingly, the angle γ between probe 1 and z'' can be expressed by $\alpha - \theta + \beta$; meanwhile, the angle between probe 2 and z'' shall be $\gamma - \pi/2$. Correspondingly, the phase modulations of the two probe components can be written as

$$\varphi_1 = \frac{2\pi L}{\lambda}(\Delta n_{z''}\cos^2\gamma + \Delta n_{y''}\sin^2\gamma), \quad (3)$$

and

$$\varphi_2 = \frac{2\pi L}{\lambda}(\Delta n_{y''}\cos^2\gamma + \Delta n_{z''}\sin^2\gamma). \quad (4)$$

As a result, the measured phase difference from THz signal and extracted from the spectral interferogram shall be

$$\varphi_m = \frac{2\pi L}{\lambda}(\Delta n_{z''} - \Delta n_{y''})(\cos^2\gamma - \sin^2\gamma). \quad (5)$$

Obviously, φ_m is proportional to the THz field $E_{\mathrm{THz}}(t)$, which means the measured waveform will be independent of α, β, and γ.

In an original CP-SI [19], the α-BBO plate is set in front of the EOC between M1 and M2 as shown in Fig. 1. Hence, the two probe components will see the THz field but with a relative time delay τ; correspondingly, Eq. (2) can be rewritten as

$$\Delta n_{y''} = \frac{n^3}{2}E_{\mathrm{THz}}(t+\tau)r_{41}[\cos\alpha\sin^2\theta + \cos(\alpha+2\theta)]. \quad (6)$$

It is obvious that the nonzero τ makes φ_m be α–dependent, thereby no longer proportional to the THz field $E_{\mathrm{THz}}(t)$. In other words, in this design, φ_m is only proportional to $E_{\mathrm{THz}}(t)$ by choosing proper α so that φ_1 or φ_2 becomes zero.

3. RESULTS AND DISCUSSIONS

According to Eq. (5), if we rotate the EOC, we can find the dependence of the measured phase induced by THz electric field on the crystal's azimuthal angle α in our improved CP-SI. In Fig. 3(a), the solid black squares present the peak values of the measured THz signals versus azimuthal angles α, the angles of the THz beam polarization with respect to the (001) axis of the EOC. The maximal phase values are about 0.13217, occurring at $\alpha = 58°$, 122°, 238°, and 302°. From Eqs. (1)–(5), we can estimate the peak value of the target THz field from the measured peak phase value by $\varphi_{\max} 1.76 \times n^3 E_{\mathrm{THz}} r_{41}/2$. Accordingly, the peak value of the measured THz field shall be 2.21 kV/cm. Here, L, n, and

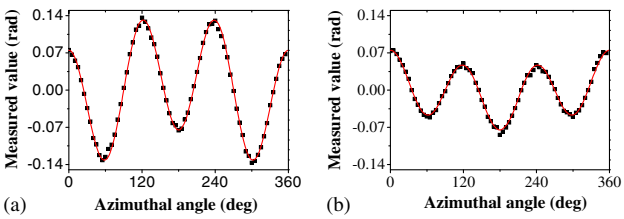

Fig. 3. Dependences of the phases induced by THz field on azimuthal angle α with (a) improved CP-SI and (b) MZ-SI.

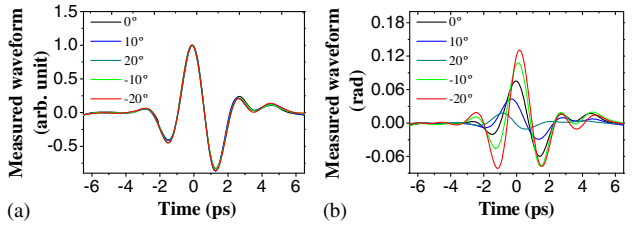

Fig. 4. Measured waveforms of THz fields for different α values with the α-BBO plate (a) after and (b) in front of the EOC.

r_{41} are the thickness, refractive index, and EO tensor of the (110) ZnTe crystal in Fig. 1. Using a traditional MZ-SI instead of our improved CP-SI, Fig. 3(b) still uses solid black squares for the peak values of the measured THz signals versus α and red line for corresponding theoretical fitting. We find the maximal values are about 0.07337 rad, about 1/1.80 of 0.13217, the value with improved CP-SI, occurring at $\alpha = 0°$ or 180°. All these experimental results agree with our theoretical fitting (red lines) very well.

Figure 4 presents the α-dependence of measured waveforms with the α-BBO plate (a) after and (b) in front of the EOC for different α values, −20°, −10°, 0°, 10°, and 20° when $\tau = 1$ ps. In Fig. 4(a) with the α-BBO plate after the EOC, all the normalized waveforms are well coincident for the different azimuthal angles α, which verifies our prediction that the measured waveform is independent of α. However, if we move the α-BBO plate in front of the EOC, Fig. 4(b) shows there are obvious differences among the waveforms for different α. We attribute the independence in Fig. 4(a) to there being no time delay induced ($\tau = 0$ ps) between the two components of the probe beam when phase modulated by the target THz field. So we can conclude that if the α-BBO plate is set before the EOC, the distortionless THz waveform is only available when $\alpha = 0°$ or 180° so that one of the two polarization components goes through the EOC without any THz phase modulation. However, if the α-BBO plate is set after the EOC, the distortion of the THz waveform for different α values will never occur from the measurements, which makes the EOC arranged more easily and the results more reliable.

Figure 5(a) presents the measured normalized THz signal with our improved CP-SI in single-shot mode (blue line); meanwhile, it also shows the normalized signals with traditional multishot scan EOS for calibration (black line) and with

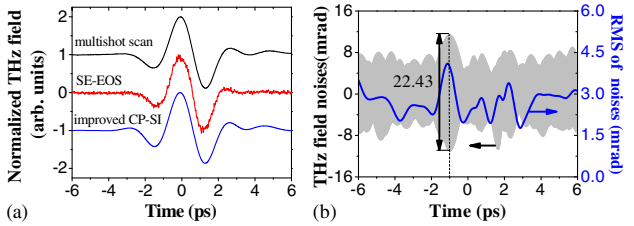

Fig. 5. (a) Normalized THz waveforms measured by three methods: traditional multi-shot scan (black line), SE-EOS averaging over 100 shots (red line), and improved CP-SI (blue line); (b) the recorded THz field noises by using improved CP-SI (gray area) and the RMS statistics over 100 shots (blue line).

spectral encoding EOS (SE-EOS) [7] (red line) for comparisons. We can see the blue line agrees with the black line very well. However, even averaging over 100 shots, the red line is still much noisier than the blue line. Figure 5(b) focuses on the recorded THz field noises by using improved CP-SI (gray area) and the RSM statistics (blue line). Here, we successively recorded the THz waveforms for 100 times, then statistically analyzed the 100 data at every sample temporal point. The gray area presents the time-dependent fluctuating region of the recoded data at the temporal region [−6 ps, 6 ps], where the maximal fluctuation is 22.43 mrad at the temporal point 1.0 ps. The blue line exhibits the corresponding time-dependent RMS values, which have an average value of about 2.7 mrad. The peak-peak value of the measured THz signal is estimated at 0.2399 rad, so the SNR of the blue line of Fig. 5(a) is about 88.85.

Figure 6 is extracted from the measurements with traditional MZ-SI [19] in order to make a comparison with our improved CP-SI. In the MZ-SI, the chirped probe is split by a beam splitter into two. One, with the phase modulation from the THz field with the EOC, is known as the signal beam, while the other without being modulated is called the reference, so they propagate non-collinearly. In Fig. 6, the measurements are made under the same optical configuration and pump source to generate THz radiation, like those in Fig. 5. Figure 6(a) shows normalized THz waveforms by traditional multi-shot scan (black line) and MZ-SI (blue line). Similar to Fig. 5(a), here we take the black line as the standard, too. Obviously, there exist some discrepancies between the black line and the blue line, especially in the temporal region [−6 ps, −3 ps], which we attribute to be the poor SNR of the blue line. Also similar to Fig. 5(b), we statistically analyze the measured noises by successively recording the THz waveforms for 100 times. The gray area of Fig. 6(b) presents the time-dependent fluctuating region of the recorded data, where it is easy to figure out that the maximal fluctuation is 120.1 mrad at the temporal point 0.9736 ps. Simultaneously, we calculate each RMS from the 100 data at each sampling point and show the RMS values with a blue line, which has an average of about 19.2 mrad. The maximal peak-peak value of the measured THz signal is around 0.1498 rad. Consequently, the SNR of the blue line in Fig. 6(a) is about 7.80. From the analyses above, we can conclude that our improved CP-SI can promote SNR from the traditional MZ-SI by a factor of ∼11.4. We have also moved the α-BBO plate in front of the EOC to record the signal with

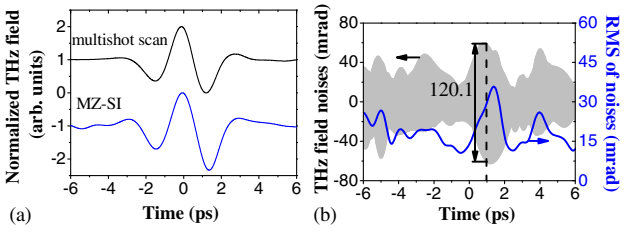

Fig. 6. (a) Normalized THz waveforms measured by traditional multi-shot scan (black line) and MZ-SI (blue line); (b) the recorded THz field noises by using MZ-SI (gray area) and the RMS statistics (blue line).

CP-SI design [19], and we can find that the RMS value of the measured noises is 3.0 mrad, very close to 2.7 mrad, that with improved CP-SI. However, the peak-peak value of the measured THz signal is about 0.1366 rad, about 1/1.75. Accordingly, the measured SNR with improved CP-SI is about 1.95 times of that with original CP-SI, which shall be attributed to higher peak-peak value of the measured THz signal obtainable with improved CP-SI.

4. CONCLUSIONS

Summarily, our improved CP-SI can promote the measured SNR by a factor of ∼11.4 over the MZ-SI, and ∼1.95 over the CP-SI. Here, improved CP-SI needs only a single probe beam through the THz EO sensor, and the spectral interference occurs between the two orthogonal polarization components of the probe with a relative time delay generated with only a birefringent plate after the EO sensor. Our experiments show this design can not only effectively suppress the noises usually suffered in a non-common-path interferometer, but also avoid the dependence of the measured waveforms on the orientation of the THz EO sensor in CP-SI. In our improved CP-SI, all used optical components are standard components, so it is very cost-effective and easy to be implemented. The measured single-shot SNR is up to 88.85. All above features mean that the interferometer is quite qualified for applications where strong THz pulses, usually with single-shot or low repetition rate, are indispensable.

Funding. National Natural Science Foundation of China (NSFC) (61490710, 61775142, 61705132); Science and Technology Planning Project of Guangdong Province (2016B050501005); Specialized Research Fund for the Shenzhen Strategic Emerging Industries Development (JCYJ20150324141711651, JCYJ20150525092941064, JCYJ20170412105812811).

REFERENCES

1. X. Zhang, A. Shkurinov, and Y. Zhang, "Extreme terahertz science," Nat. Photonics **11**, 16–18 (2017).
2. D. M. Mittleman, M. Gupta, R. Neelamani, R. G. Baraniuk, J. V. Rudd, and M. Koch, "Recent advances in terahertz imaging," Appl. Phys. B **68**, 1085–1094 (1999).
3. Z. Jiang, F. G. Sun, Q. Chen, and X. Zhang, "Electro-optic sampling near zero optical transmission point," Appl. Phys. Lett. **74**, 1191–1193 (1999).
4. X. Pan, Y. Cai, X. Zeng, X. Lu, D. Zhang, J. Li, H. Chen, and S. Xu, "Modified THz electro-optic sampling for high optical modulation depth, large dynamical range and low background noises," Opt. Lett. **39**, 3778–3781 (2014).
5. G. Sharma, K. Singh, I. Al-Naib, R. Morandotti, and T. Ozaki, "Terahertz detection using spectral domain interferometry," Opt. Lett. **37**, 4338–4340 (2012).
6. M. Teo Stephanie, K. Ofori-Okai Benjamin, A. Werley Christopher, and A. Nelson Keith, "Single-shot THz detection techniques optimized for multidimensional THz spectroscopy," Rev. Sci. Instrum. **86**, 051301 (2015).
7. Z. Jiang and X. Zhang, "Electro-optic measurement of THz field pulses with a chirped optical beam," Appl. Phys. Lett. **72**, 1945–1947 (1998).
8. G. P. Wakeham and K. A. Nelson, "Dual-echelon single-shot femtosecond spectroscopy," Opt. Lett. **25**, 505–507 (2000).
9. K. Y. Kim, B. Yellampalle, A. J. Taylor, G. Rodriguez, and J. H. Glownia, "Single-shot terahertz pulse characterization via

two-dimensional electro-optic imaging with dual echelons," Opt. Lett. **32**, 1968–1970 (2007).
10. J. Shan, A. S. Weling, E. Knoesel, L. Bartels, M. Bonn, A. Nahata, G. A. Reider, and T. F. Heinz, "Single-shot measurement of terahertz electromagnetic pulses by use of electro-optic sampling," Opt. Lett. **25**, 426–428 (2000).
11. Y. Kawada, T. Yasuda, A. Nakanishi, K. Akiyama, and H. Takahashi, "Single-shot terahertz spectroscopy using pulse-front tilting of an ultra-short probe pulse," Opt. Express **19**, 11228–11235 (2011).
12. F. D. J. Brunner, J. A. Johnson, S. Grübel, A. Ferrer, S. L. Johnson, and T. Feurer, "Distortion-free enhancement of terahertz signals measured by electro-optic sampling. I. Theory," J. Opt. Soc. Am. B **31**, 904–910 (2014).
13. J. A. Johnson, F. D. J. Brunner, S. Grübel, A. Ferrer, S. L. Johnson, and T. Feurer, "Distortion-free enhancement of terahertz signals measured by electro-optic sampling. II. Experiment," J. Opt. Soc. Am. B **31**, 1035–1040 (2014).
14. S. P. Jamison, A. M. Macleod, W. A. Gillespie, and D. A. Jaroszynski, "High-temporal-resolution, single-shot characterization of terahertz pulses," Opt. Lett. **28**, 1710–1712 (2003).
15. Z. Jin, A. Wada, J. H. Shin, N. Yugami, and R. Kodama, "A single-shot terahertz time-domain," J. Phys. Conf. Ser. **688**, 012040 (2016).
16. N. H. Matlis, G. R. Plateau, J. V. Tilborg, and W. P. Leemans, "Single shot spatiotemporal measurements of ultrashort THz waveforms using temporal electric-field cross correlation," J. Opt. Soc. Am. B **28**, 23–27 (2011).
17. A. Ibrahim, G. Sharma, K. Singh, and T. Ozaki, "Terahertz detection based on spectral-domain interferometry using Mach-Zehnder interferometer," J. Infrared Millimeter Terahertz Waves **37**, 837–845 (2016).
18. G. Sharma, K. Singh, A. Ibrahim, I. Al-Naib, R. Morandotti, F. Vidal, and T. Ozaki, "Self-referenced spectral domain interferometry for improved signal-to-noise measurement of terahertz radiation," Opt. Lett. **38**, 2705–2707 (2013).
19. S. Zheng, X. Pan, Y. Cai, Q. Lin, Y. Li, S. Xu, J. Li, and D. Fan, "Common-path spectral interferometry for single-shot terahertz optics-electro detection," Opt. Lett. **42**, 4263–4266 (2017).
20. J. Hebling, K. Yeh, M. Hoffmann, B. Bartal, and K. Nelson, "Generation of high-power terahertz pulses by tilted-pulse-front excitation and their application possibilities," J. Opt. Soc. Am. B. **25**, B6–B19 (2008).
21. S. Zheng, Y. Cai, X. Pan, X. Zeng, J. Li, Y. Li, T. Zhu, Q. Lin, and S. Xu, "Two-step phase-shifting SPIDER," Sci. Rep. **6**, 33837 (2016).
22. P. C. M. Planken, H. K. Nienhuys, H. J. Bakker, and T. Wenckebach, "Measurement and calculation of the orientation dependence of terahertz pulse detection in ZnTe," J. Opt. Soc. Am. B **18**, 313–317 (2001).